Earth and Planetary Science Letters 351–352 (2012) 258–269

Contents lists available at SciVerse ScienceDirect

Earth and Planetary Science Letters

journal homepage: www.elsevier.com/locate/epsl

Giant magnetofossils and hyperthermal events

Liao Chang [a,1], Andrew P. Roberts [a,b,*], Wyn Williams [c], John D. Fitz Gerald [b], Juan C. Larrasoaña [b,d], Luigi Jovane [a,e], Adrian R. Muxworthy [f]

[a] School of Ocean and Earth Science, National Oceanography Centre, University of Southampton, European Way, Southampton SO14 3ZH, UK
[b] Research School of Earth Sciences, The Australian National University, Canberra, ACT 0200, Australia
[c] Grant Institute of Earth Science, University of Edinburgh, Kings Buildings, West Mains Road, Edinburgh EH9 3JW, UK
[d] Instituto Geológico y Minero de España, Unidad de Zaragoza, Manuel Lasala 44 9B, 13 Zaragoza 50006, Spain
[e] Instituto Oceanográfico da Universidade de São Paulo, Praça do Oceanográfico, 191 - São Paulo, SP 05508–120, Brazil
[f] Department of Earth Science and Engineering, Imperial College London, South Kensington Campus, London SW7 2AZ, UK

ARTICLE INFO

Article history:
Received 28 March 2012
Received in revised form
10 July 2012
Accepted 16 July 2012
Editor: J. Lynch-Stieglitz

Keywords:
giant magnetofossils
hyperthermal
eukaryote
magnetotactic bacteria

ABSTRACT

Magnetotactic bacteria biomineralize magnetic minerals with precisely controlled size, morphology, and stoichiometry. These cosmopolitan bacteria are widely observed in aquatic environments. If preserved after burial, the inorganic remains of magnetotactic bacteria act as magnetofossils that record ancient geomagnetic field variations. They also have potential to provide paleoenvironmental information. In contrast to conventional magnetofossils, giant magnetofossils (most likely produced by eukaryotic organisms) have only been reported once before from Paleocene-Eocene Thermal Maximum (PETM; 55.8 Ma) sediments on the New Jersey coastal plain. Here, using transmission electron microscopic observations, we present evidence for abundant giant magnetofossils, including previously reported elongated prisms and spindles, and new giant bullet-shaped magnetite crystals, in the Southern Ocean near Antarctica, not only during the PETM, but also shortly before and after the PETM. Moreover, we have discovered giant bullet-shaped magnetite crystals from the equatorial Indian Ocean during the Mid-Eocene Climatic Optimum (~40 Ma). Our results indicate a more widespread geographic, environmental, and temporal distribution of giant magnetofossils in the geological record with a link to "hyperthermal" events. Enhanced global weathering during hyperthermals, and expanded suboxic diagenetic environments, probably provided more bioavailable iron that enabled biomineralization of giant magnetofossils. Our micromagnetic modelling indicates the presence of magnetic multi-domain (i.e., not ideal for navigation) and single domain (i.e., ideal for navigation) structures in the giant magnetite particles depending on their size, morphology and spatial arrangement. Different giant magnetite crystal morphologies appear to have had different biological functions, including magnetotaxis and other non-navigational purposes. Our observations suggest that hyperthermals provided ideal conditions for giant magnetofossils, and that these organisms were globally distributed. Much more work is needed to understand the interplay between magnetofossil morphology, climate, nutrient availability, and environmental variability.

1. Introduction

Magnetic minerals, particularly magnetite (Fe_3O_4), are common biomineralization products. Fossilized biogenic magnetic minerals produced by magnetotactic bacteria, which are known as magnetofossils, provide important records of past microbial ecosystems, environmental change, and geomagnetic field behaviour (Kopp and Kirschvink, 2008). Recent discovery of large and novel biogenic magnetite crystals produced by presumably eukaryotic organisms during the Paleocene-Eocene Thermal Maximum (PETM) — the most extreme Cenozoic global warming event (Kennett and Stott, 1991; Zachos et al., 2008) — demonstrates the impact of global warming on ecosystems (Schumann et al., 2008). It also raises the question of whether biomineralization of such giant magnetofossils is linked to short-lived extreme warming events ("hyperthermals"). We here address this question through detailed transmission electron microscope (TEM) analysis of magnetofossils extracted from deep-sea sediments of different age (Fig. 1), particularly across hyperthermal events. We also carried out micromagnetic modelling to constrain the potential biological functions of these giant magnetite crystals.

* Corresponding author at: Research School of Earth Sciences, The Australian National University, Building 142, 61 Mills Road, Canberra, ACT 0200, Australia. Tel.: +61 2 61252487.
E-mail address: andrew.roberts@anu.edu.au (A.P. Roberts).
[1] Now at: Paleomagnetic Laboratory 'Fort Hoofddijk', Department of Earth Sciences, Utrecht University, Budapestlaan 17, 3584 CD Utrecht, The Netherlands.

0012-821X/$ - see front matter © 2012 Elsevier B.V. All rights reserved.
http://dx.doi.org/10.1016/j.epsl.2012.07.031

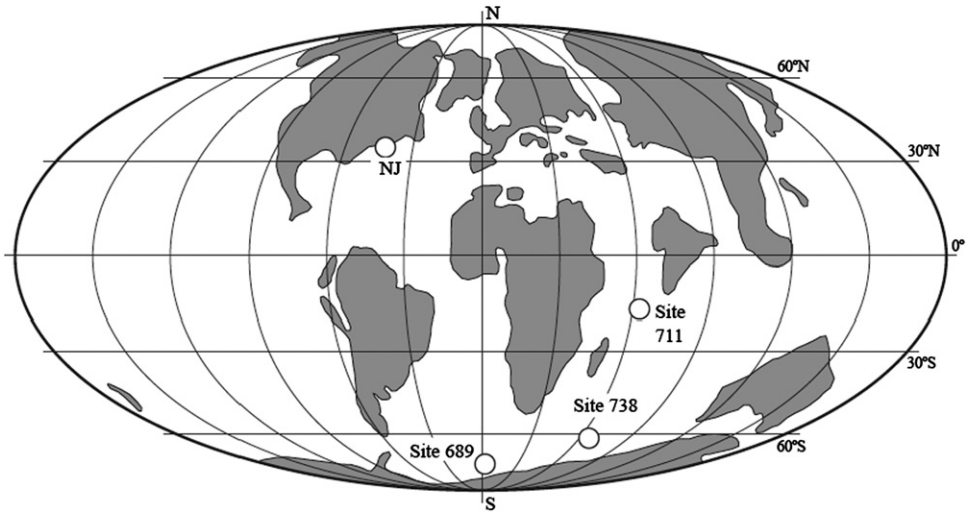

Fig. 1. Location of the studied ODP sites (738, 711 and 689) from the Indian and Southern Oceans and the New Jersey (NJ) site from which Schumann et al. (2008) reported giant magnetofossils from the PETM. The map is a reconstruction at the Paleocene-Eocene boundary.

2. Methods

We analysed pelagic marine sediments from Ocean Drilling Program (ODP) sites 738, 711 and 689 (Fig. 1). Hole 738C was cored on the Antarctic margin, southern Kerguelen Plateau (62°42, 54'S; 82°47, 25'E; 2,253 m water depth (1,750 m paleo water depth)). Hole 711 A was cored on Madingley Rise in the equatorial Indian Ocean (2°44.56'S; 61°09.78'E; 4,428 m water depth). Hole 689D was cored on Maud Rise, Weddell Sea, Antarctica (64°31.01'S; 03°06.00–03°06.30'E; 2,080 m water depth (paleo depth 1,600 m)). The studied sediments are white calcareous foraminiferal nannofossil chalks. The magnetic properties of the sediments are dominated by single-domain (SD) magnetite, which are due to the presence of magnetofossil chains produced by magnetotactic bacteria (Roberts et al., 2011; Larrasoaña et al., 2012).

We modified the methods of Stoltz et al. (1986) and Hesse (1994) to obtain magnetic mineral extracts and to prepare TEM samples. First, ~1 g of untreated sediment was mixed with ~50 ml of distilled water in a glass beaker. We did not dissolve carbonates with acid or sieve samples to remove large nannofossils. The beaker was then placed in an ultrasonic bath for 5 minutes to disperse the particles. We used the electromagnet of a Frantz isodynamic magnetic separator with a glass tube placed between the pole pieces to concentrate magnetic minerals and to reduce the abundance of non-magnetic materials (e.g., nannofossils, clays, salts, etc.). The glass tube (with stopcock at the base) was filled with distilled water with air at the top. The electromagnet was then switched on to produce a large magnetic field around the tube. Sediment solution was added slowly into the tube from the top. Sediment gradually deposited at the bottom of the tube. Some magnetic minerals were trapped onto the walls of the glass tube. After ~30 minutes, the stopcock at the bottom of the tube was opened and material deposited at the bottom was removed. This procedure was repeated until all of the sediment solution had been subjected to magnetic extraction. The magnetic minerals that attached to the tube walls were washed with a small amount of distilled water. The solution with separated magnetic minerals was transferred into a test tube, which was placed next to a rare earth magnet. After several hours, clear water and heavy non-magnetic materials that deposited at the bottom of the container were gently removed with a pipette. The small amount of material that concentrated beside the magnet was transferred to a copper TEM grid, which had previously been carbon coated. The TEM grid was floated on top of the solution with the carbon side facing down and a rare earth magnet was then suspended ~1 cm above the TEM grid to attract magnetic particles for ~30 minutes. Magnetic extracts were viewed and analysed using a Philips CM300 TEM operated at 300 kV in the Research School of Earth Sciences, Australian National University. The TEM is equipped with an EDAX Phoenix retractable X-ray detector (ultra-thin window) and a Gatan 694 slow-scan digital camera.

The micromagnetic model used is a hybrid finite element/boundary integral (FEBI) model (e.g., Schrefl, 1999; Williams et al., 2006, 2010). The modelled crystal geometries were created and then meshed with arbitrarily shaped tetrahedral elements using the CUBIT (cubit.sandia.gov) software package. The magnetization was evaluated at the nodes of the tetrahedral vertices. To determine the equilibrium magnetic structure, we used a combined algorithm (Muxworthy and Williams, 2006; Williams et al., 2006, 2010). Initially, we used a conjugate-gradient energy minimization solver to rapidly find a local energy minimum. The initial estimate was refined by solving the dynamic Landau-Lifshitz-Gilbert equation to provide a robust equilibrium magnetic structure by minimizing the torque at each node. Room-temperature parameters for magnetite were used: saturation magnetization, $M_s = 4.8 \times 10^5\ \mathrm{Am}^{-1}$, exchange constant, $A = 1.34 \times 10^{-11}\ \mathrm{Jm}^{-1}$ (Heider and Williams, 1988), and magnetocrystalline anisotropy constant, $K_1 = 1.24 \times 10^4\ \mathrm{Jm}^{-3}$ (Fletcher and O'Reilly, 1974). In all models the $<1\,1\,1>$ crystallographic direction was assumed to be parallel to the elongation axis, which is consistent with observations on magnetite magnetosomes (Matsuda et al., 1983; Mann et al., 1984; Buseck et al., 2001; Abraçado et al., 2010).

3. Results

All of the studied magnetic separates contain abundant conventional magnetofossils, including hexagonal prisms, cuboidal and bullet-shaped morphologies (Fig. 2). Selected-area electron diffraction (SAED), energy dispersive X-ray spectra (EDS) (Fig. 3) and high-resolution TEM (HR-TEM) imaging indicate a magnetite composition for the analysed particles. These small magnetite crystals (~40–200 nm) were sometimes observed in short chains (Fig. 2). Detailed rock magnetic analyses also confirm the preservation of conventional magnetofossils across the PETM section (Larrasoaña et al., 2012) and throughout the Eocene at Site 738

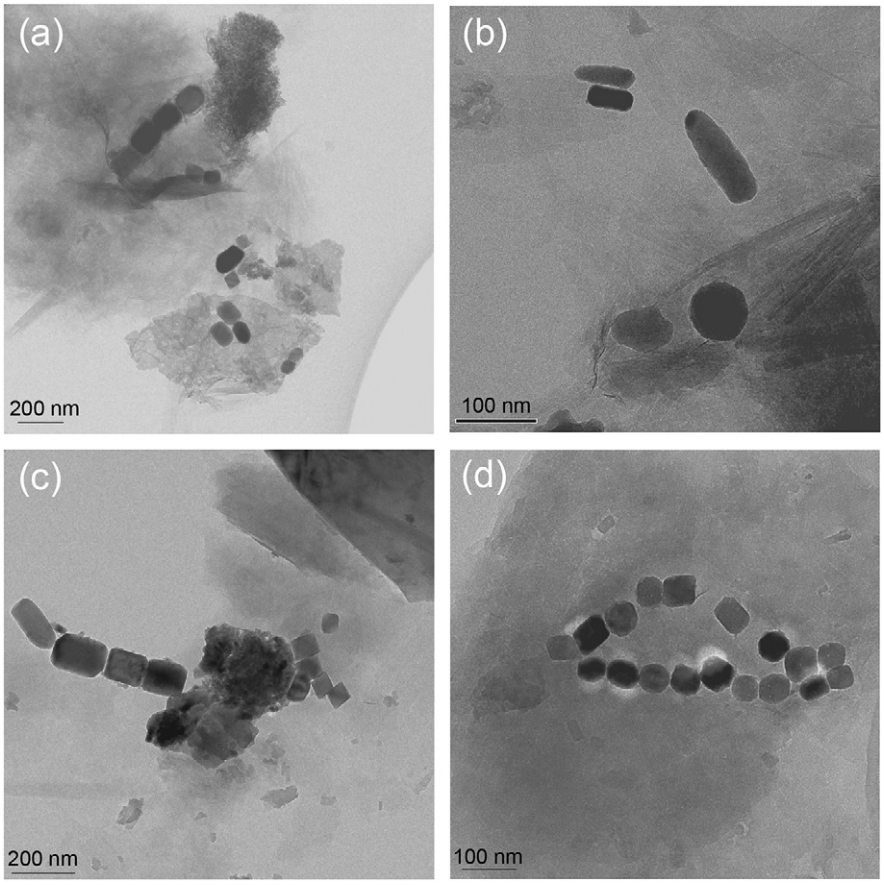

Fig. 2. TEM images of conventional magnetofossils from two deep-sea sediment cores. (a) A short magnetofossil chain with hexagonal prisms and other magnetite clusters extracted from ODP Hole 711A (during MECO), (b) isolated bullet-shaped magnetite crystals extracted from Hole 711A (during MECO), (c) short magnetofossil chains with hexagonal prisms and octahedral magnetite crystals extracted from Hole 738C (after the PETM), and (d) magnetite particle clusters extracted from Hole 738C (during the PETM).

(Roberts et al., 2011). In addition to conventional magnetofossils, we identified several types of giant magnetofossils. SAED, EDS and HR-TEM results from these giant particles indicate that they consist of magnetite (Figs. 3–7), with pure chemical composition and lattice perfection, which is consistent with a biological origin for the magnetite. Low-temperature magnetic measurements on the same samples (Roberts et al., 2012) contain evidence for a Verwey transition, which confirms the presence of magnetite. Low-temperature magnetic data also indicate partial maghemitization of magnetite crystals. All observed giant crystals were analysed with EDS; most were further analysed with SAED to confirm their magnetite composition.

The observed giant magnetofossil morphologies include previously reported spindle-like, elongated prismatic (needle-like), and possible spearhead-shaped crystals. The spindle-like crystals are tapered toward their ends, with a length-to-width ratio up to ~10 and length up to 1.7 μm (Fig. 4a). The extremely elongated prismatic, defect-free crystals have a needle-like morphology with length-to-width ratios ranging from 6 to 16 and lengths up to 1.6 μm (Fig. 5, 6). Possible spearhead-like crystals and their crystal fragments are observed (e.g., Fig. 5c), although this evidence is ambiguous and we cannot be sure of the presence of spearhead morphologies. Nevertheless, the needle- and spindle-shaped crystal morphologies are identical to those observed by Schumann et al. (2008). We have also discovered new giant bullet-shaped crystals (Figs. 4c, 5a, 7). The giant bullet-shaped crystals have similar shapes to those of smaller conventional bullet-shaped magnetosomes (Fig. 2b) (e.g., Petersen et al., 1986; Lins et al., 2007; Li et al., 2010), but with lengths up to 3 μm. Giant bullet- and needle-like crystals are possibly large counterparts to common magnetofossil morphologies. These larger counterparts of bacterial bullet-shaped crystals could, therefore, be of bacterial origin. While some bacteria have cells that are large enough to accommodate such large bullet crystals, bacteria could not cleave such large single crystals during cell division. Daughter cells would, therefore, need to grow single crystals, unlike the case of magnetosome chains that can split into two halves during cell division (Katzmann et al., 2011). We also identified porous single crystals (Fig. 4d, 6c) that can resemble clustered ultrafine particles. Tilting under TEM indicates that these particles are magnetite single crystals, with good crystallinity and well-pronounced crystal faces, but with a porous structure (Fig. 4d). The structures of these large magnetite crystals may be produced as a result of dissolution effects (Vali and Kirschvink, 1989). However, the crystals also have sharp edges and patterned layers within the crystal body (Fig. 4d), which are different from dissolved magnetofossil crystals (Vali and Kirschvink, 1989). Furthermore, clear preservation of crystalline fine-grained conventional magnetosomes (Fig. 2; Larrasoaña et al., 2012) is difficult to reconcile with partial dissolution of the observed large porous magnetite crystals.

4. Discussion

4.1. Giant magnetofossils and hyperthermals

We summarize our observations of giant magnetofossils in Table 1. There is only one previous report of giant biogenic magnetite, which is restricted to the PETM section at Ancora, New Jersey.

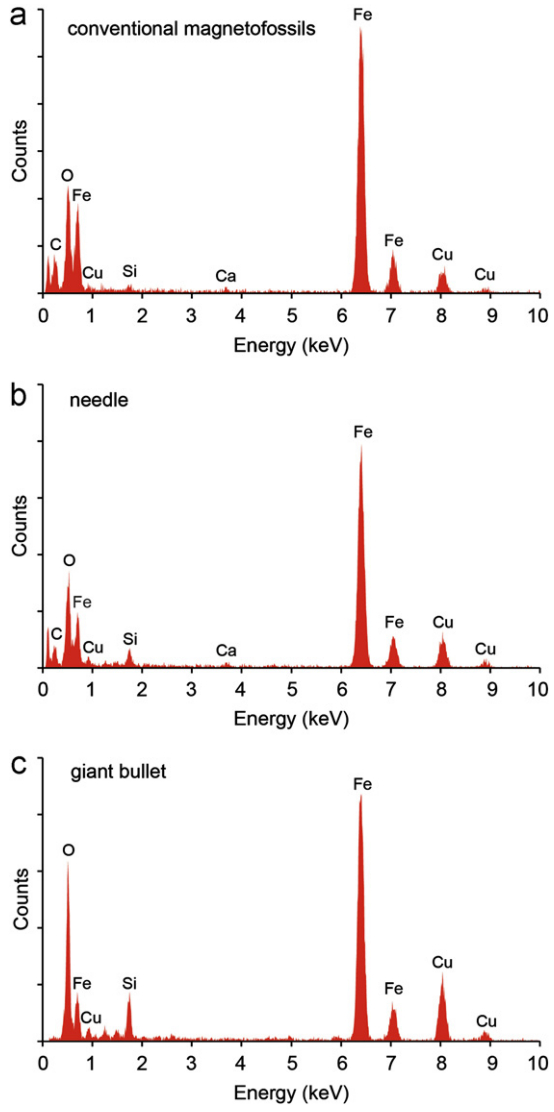

Fig. 3. Selected energy dispersive X-ray absorption spectra for (a) conventional magnetofossils, (b) a needle-like crystal, and (c) a giant bullet-shaped crystal. The analysed crystals always have strong iron and oxygen peaks, which is consistent with the composition of biogenic magnetite. Cu peaks originate from the TEM grid. C is from the carbon film of the TEM grid. The small Ca signal originates from large $CaCO_3$ particles near the analysed particles. The Si peaks arise from the many small, thin siliceous bodies scattered across the TEM grid.

Schumann et al. (2008) hypothesized that such novel gigantism in biogenic magnetite is produced by dramatic changes in weathering and sedimentation patterns driven by severe global warming (e.g., Bowen et al., 2004). In the subtropical paleolatitudes of the Atlantic costal plain, development of a thick suboxic zone with high iron bioavailability is argued to have driven diversification of magnetite-forming eukaryotes (Schumann et al., 2008). We document identical giant magnetofossils from deep-sea environments. In this pelagic setting, it is iron fertilization, associated with increased eolian dust flux, that appears to have resulted in increased surface water productivity and organic carbon export to the seafloor, which provided both nutrients for microbial metabolism and gave rise to suboxic diagenetic conditions that released labile iron under mild iron-reducing conditions to fuel iron biomineralization (Roberts et al., 2011; Larrasoaña et al., 2012).

In addition, we find that giant biogenic magnetite occurred not only during the PETM (Fig. 4), but also before (Fig. 5) and after the PETM (Fig. 6). Although bioturbation can rework material down-section and magnetite-producing bacteria can live within sediments (Tarduno and Wilkison, 1996; Bazylinski and Frankel, 2004; Flies et al., 2005; Kopp and Kirschvink, 2008), Larrasoaña et al. (2012) demonstrated that magnetofossil abundance coincided precisely with variations in eolian iron input. This suggests that the biogenic magnetite formed at or close to the sediment-water interface (Larrasoaña et al., 2012). This evidence suggests that the giant magnetofossils have not been stratigraphically displaced and that they therefore were present before and after the PETM. Significant sea surface warming and environmental change, as indicated by the TEX_{86} paleothermometer and by high abundances of a subtropical dinoflagellate cyst at high latitudes, preceded the light carbon injection associated with the PETM by several thousand years (Sluijs et al., 2007). Thus, global warming that preceded the PETM may have played a role in the evolution and distribution of the giant magnetite-producing organisms.

We also identified giant bullet-shaped magnetite during another hyperthermal event – the Mid-Eocene Climatic Optimum (MECO; Bohaty and Zachos, 2003; Jovane et al., 2007) (Fig. 7). This suggests a wider association of giant biogenic magnetite with hyperthermal events. We also analysed multiple samples from different localities throughout the intervening Eocene interval, but found no evidence of giant magnetofossils in these samples, although conventional magnetofossils are abundant (e.g., Roberts et al., 2011). It is possible that low concentrations of giant magnetofossils may preclude their identification during these more 'normal' greenhouse climatic periods, and we cannot conclude that they were absent in these periods. Nevertheless, currently available evidence indicates that biomineralization of giant magnetofossils was closely coupled to hyperthermal events. The unusual enhanced growth of giant magnetofossils was probably caused by significant ecological changes during hyperthermals (Kopp et al., 2007, 2009; Schumann et al., 2008) and their preservation in the geological record is probably due to thick suboxic, but not anoxic, sediment sequences in which iron was plentifully available to enable magnetite biomineralization (Roberts et al., 2011). Enhanced global weathering likely due to enhanced seasonality and concomitant terrestrial environmental changes is likely to have increased the supply of dissolved iron to pelagic marine environments, which would have also removed a normal limitation for iron biomineralization. Conventional biogenic magnetite is widely reported in PETM sediments from New Jersey (Lippert and Zachos, 2007; Kopp et al., 2007, 2009) in addition to giant magnetofossils (Schumann et al., 2008). Widespread occurrence of biogenic SD magnetite in these settings suggests that comet impact is not the most likely explanation for the presence of abundant SD magnetite within the PETM (Kent et al., 2003; Cramer and Kent, 2005).

We observe variable relative abundance and morphological patterns for different giant magnetofossils through the PETM (Table 1). For example, we identified abundant giant bullet-shaped and spindle-like magnetite crystals before the PETM, but no evidence of needle-like crystals before the PETM. During the PETM, we observe all types of giant magnetofossils, including needle-, spindle-, and bullet-shaped crystals. After the PETM, the dominant morphology is needle-like, with rare occurrences of giant bullet crystals. We found no evidence of spindle-like or possible spearhead-like crystals after the PETM. Moreover, we observed the most elongated needle-like crystals (length-to-width ratio=16) and the largest giant bullet-shaped crystal (3 μm) during the PETM. The average elongation of needle-like crystals is slightly larger during the PETM (length-to-width ratio=~10) compared to that after the PETM (~9). We only identified giant bullet-shaped magnetofossils during the MECO event (average size=2.3×0.5 μm). Our data support the conclusion of Schumann et al. (2008) that gigantism in biogenic magnetite is enhanced during extremely warm climates.

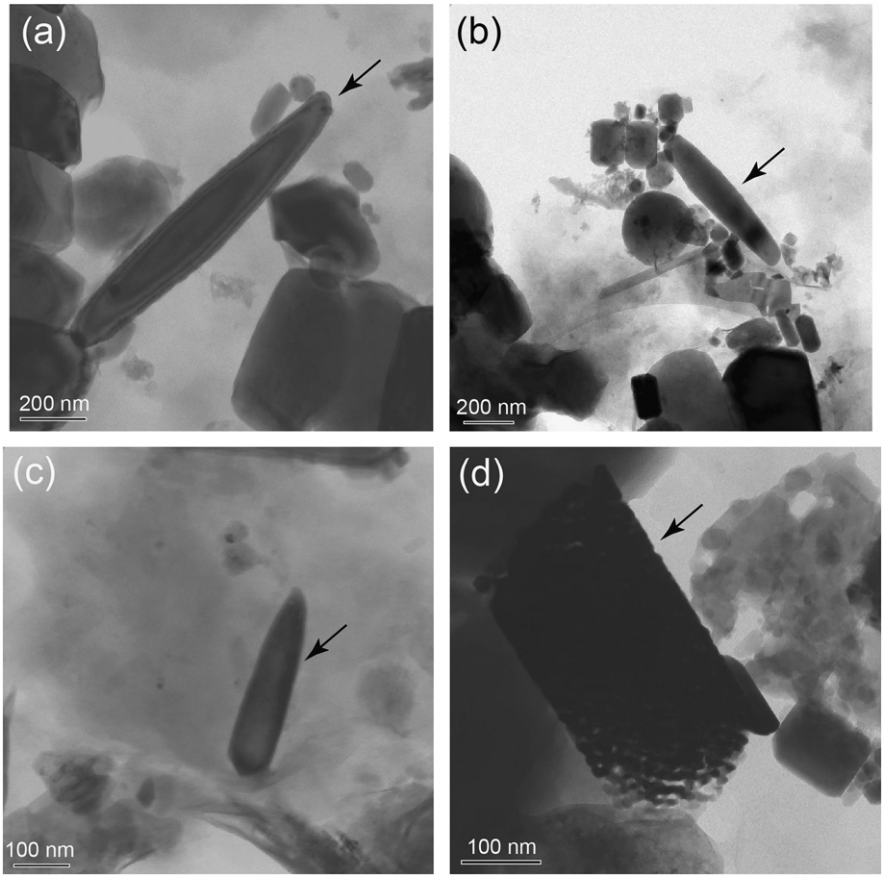

Fig. 4. TEM images of a magnetic separate for a pre-PETM sample from Hole 738C (285.63 msbf). The well-defined carbon isotope excursion associated with the PETM extends from depths of 285.5 to 284.4 mbsf at Hole 738C (Larrasoaña et al., 2012). Arrows indicate giant magnetofossils. (a) A spindle-like magnetite crystal, (b) a possible transitional morphology between spindle-like and needle-like crystals, (c) a giant bullet-shaped magnetite crystal, and (d) a porous single magnetite crystal. The sample is from ~30 cm below the onset of the PETM (285.63 msbf). Non-magnetic impurities are mainly fragments of nannofossils, silicates and clay minerals.

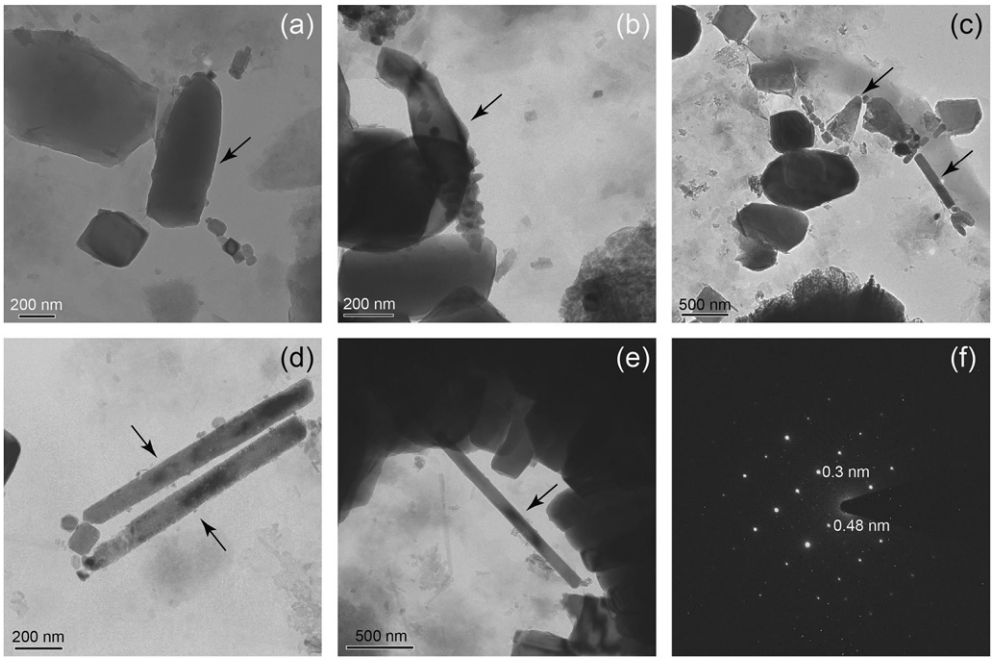

Fig. 5. TEM images of a magnetic separate from the PETM at Hole 738C (284.75 mbsf). Black arrows indicate giant magnetofossils. (a) A giant bullet-shaped magnetite crystal, (b) an irregular magnetite single crystal, (c) a possible spearhead fragment and a needle-like crystal, (d) two needle-like magnetite crystals, (e) an extremely elongated prismatic magnetite crystal, and (f) electron diffraction pattern of the elongated prismatic crystal in (e). The d-spacings of 3 Å and 4.8 Å correspond to the lattice fringes for the {2 2 0} and {1 1 1} planes in magnetite.

Table 1
Summary of analysed samples and types of giant magnetofossils identified.

ODP Hole	Section	Interval (cm)	Depth (msbf)	Period	Types of giant magnetofossils
738C	11R1	28	283.68	Pre-PETM	Spindle, giant bullet
738C	11R1	135	284.75	During PETM	Needle, giant bullet, spindle, possible spearhead
738C	11R2	73	285.63	After PETM	Needle, giant bullet
738B	5H2	101	35.01	Eocene	None
689D	11H6	21	122.21	Oligocene	None
711A	20 × 4	41	187.01	During MECO	Giant bullet

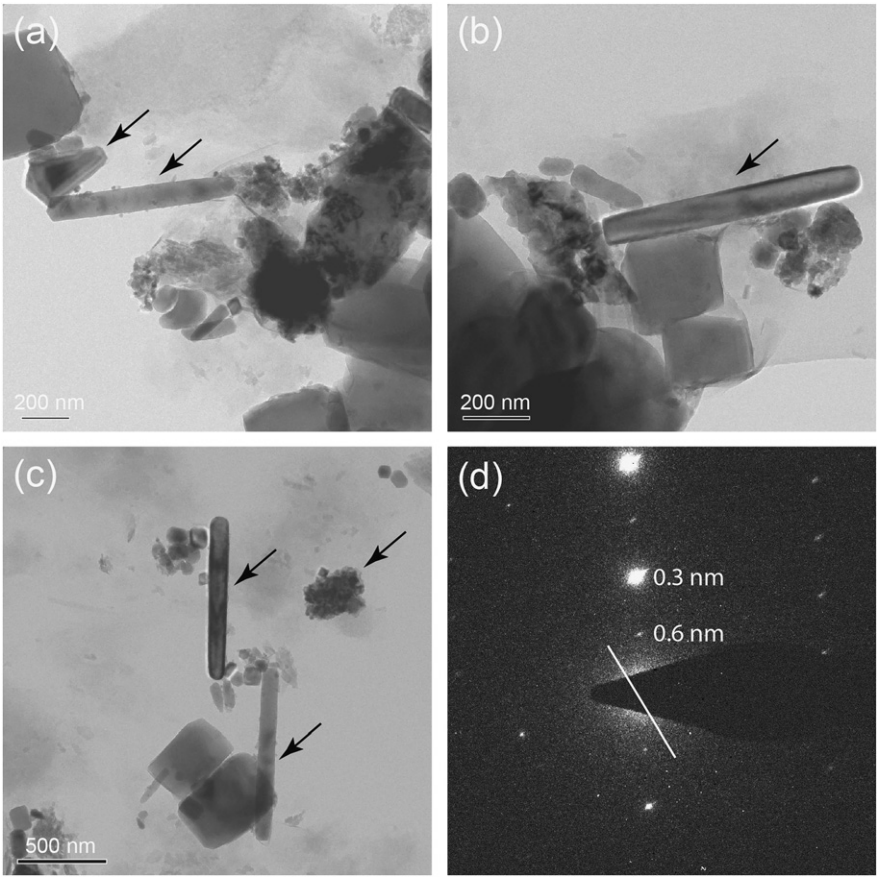

Fig. 6. (a-c) TEM images of giant magnetofossils from after the PETM at ODP Hole 738C (283.68 mbsf). (d) Electron diffraction pattern of the upper needle-like crystal in (c). The d-spacing of 3 Å corresponds to the {2 2 0} lattice fringe for magnetite. The white line in (d) represents the long axis of the corresponding needle-like crystal.

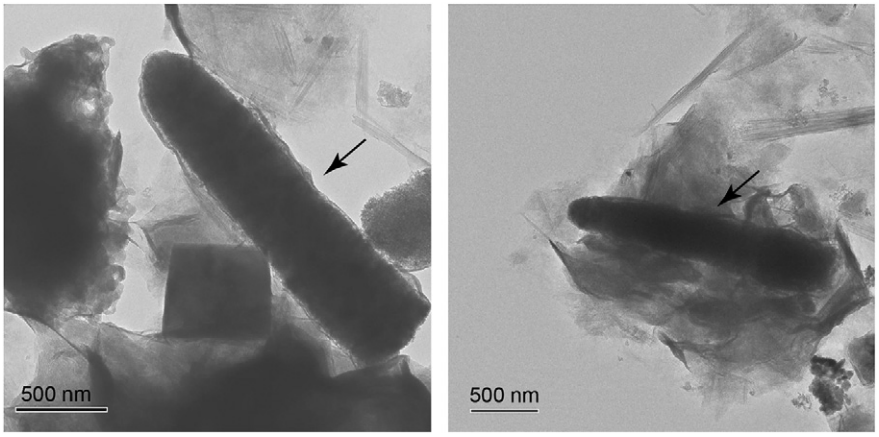

Fig. 7. TEM images of giant bullet-shaped magnetofossils during the MECO event extracted from Hole 711A (187.01 mbsf). Arrows indicate the giant bullet-shaped magnetites. The thin layer surrounding the magnetite is amorphous silica.

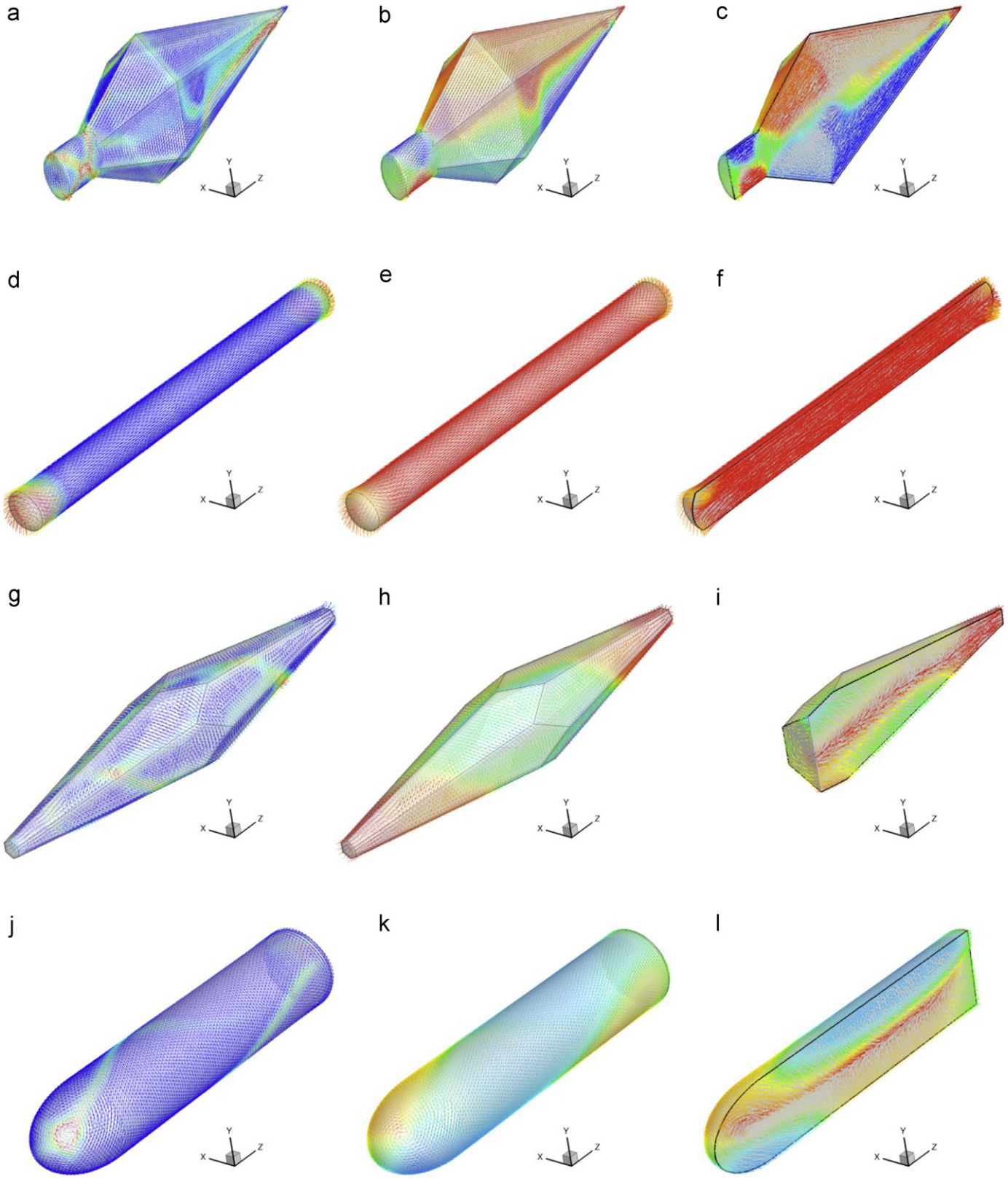

Fig. 8. Micromagnetic simulations of the magnetic domain structures of giant magnetofossils. (a-c) Complex MD structure of a spearhead-like magnetite crystal (4×1.715 μm). (d-f) SD structure of a magnetite rod (1.1×0.1 μm). (g-i) PSD-like structure of a spindle-like crystal (2.245×0.375 μm). (j-l) PSD vortex domain structure of a large giant bullet-shaped crystal (2.081×0.478 μm). In each case, the images in the left-hand column are magnetic structures with magnetic vectors coloured according to the calculated vorticity magnitude, which highlight domain walls. The magnetic structures in the middle column are coloured according to the Cartesian x, y, z directions (red = +z, blue = -z), which highlight magnetic domains. The images in the right-hand column are slices through the crystal, which reveal the magnetic structure (at the $X=0$ plane) inside the crystal. The colour scale is the same as for the middle column. The modelled SD structure in the elongated prisms (d-f) indicates that they may have been used for navigation. Complex PSD/MD structures in other giant magnetite crystals indicate that were probably not efficient for navigational purposes.

4.2. Physiological functions of giant magnetofossils

We carried out micromagnetic modelling to determine the magnetic properties of the giant magnetite crystals in order to better understand their potential physiological functions. Micromagnetic simulation of a single spearhead crystal (4×1.715 μm) reveals complex multi-domain (MD) structures with magnetic domains extending from the surface to deep inside the crystal (Fig. 8a-c). This result contrasts with previous electron holography measurements, which indicated magnetically uniform SD structures for spearheads from analysis of the external stray field (Schumann et al., 2008). However, as argued by Schumann et al. (2008), this SD pattern might reflect a metastable state imparted during the magnetic concentration process, where the magnetic particles were attracted to the pole of a strong permanent magnet. Furthermore, Schumann et al. (2008) provided evidence in their Supporting Information that the spearhead particles occur in an agglutinated configuration with spearheads pointing outward as a cellular armour, which indicates that the particles had a protective rather than navigational (magnetotaxis) function. Our micromagnetic modelling results support this evidence for a non-magnetotactic function for the spearhead crystals.

In contrast, simulation of needle-like crystals indicates SD structures (Fig. 8d-f). The body of the modelled rod has uniform magnetic moments that parallel the elongation axis. There is only a small non-uniform magnetization toward both ends of the rods. This minor deflection of magnetic moments resembles a SD flower-like structure, but the moments are twisted around the long axis to form a helical pattern (Fig. 8d-f). Nevertheless, the non-uniform magnetization only constitutes a small portion of the total magnetic moment and the whole rod has strongly SD behaviour. For spindle-like (Fig. 8g-i) and giant bullet-shaped crystals (Fig. 8j-l), modelling indicates that these crystals can be either SD or MD depending on their size and shape. A large spindle crystal (2.245×0.375 μm) has a pseudo-single domain (PSD)-like structure with a vortex core in the centre and many surface domains (Fig. 8g-i). A large giant bullet-shaped crystal (2.081×0.478 μm) also has a vortex domain structure with the vortex core within the grain and complex surface domains (Fig. 8j-l). Clearly, some isolated giant magnetite crystals are too large for efficient magnetotaxis, but we cannot exclude the possibility that some giant crystals, e.g., needle and smaller giant bullets (i.e., Fig. 4c), either as single crystals or within chains, were used for magnetotaxis.

We further modelled different spatial arrangements of giant crystals with different morphologies to test the possibility that they were used for navigation. The original arrangement of the giant magnetite spindle- and bullet-shaped crystals within the organism is not known. We therefore modelled only simple chain structures (Figs. 9–10). Although Schumann et al. (2008) provided evidence in their Supporting Information that the giant spearhead magnetites were used for defensive purposes, we modelled simple chain structures to test whether they could have been used for magnetotaxis. All multi-grain models were computed using a constrained optimization method, where only the magnetization of the central grain was allowed to vary. The magnetization of all other grains was constrained in one direction. We therefore need to only consider the nearest neighbouring interactions. This provides the maximum magnetic interaction field. The aim of the modelling was to force the central grain to have a maximum possible remanence to determine whether interactions with other particles could favour magnetotaxis. Constrained magnetizations are unlikely in reality, but they provide constraints on the optimal magnetization for such particles.

Giant spindle-like crystals have vortex structures when they are assembled in a simple linear chain with three spindle crystals (Fig. 9a). But the normalized saturation remanent magnetization (M_{rs}) increases from 0.355 for an isolated spindle to 0.505 for a nearly touching chain (Table 2), which indicates enhancement to SD structure when assembled in a chain. Simulating multiple parallel chains with eleven spindles and a small inter-particle spacing (Fig. 9b) indicates a stable SD state with M_{rs} of 0.98 (Table 2). Modelling parallel spindle chains with different inter-particle spacing (Fig. 9b-f) indicates enhancement to SD structure with decreasing inter-particle gaps (Table 2). Modelling of giant bullet-shaped magnetofossils indicates a dramatic increase in M_{rs} from only 0.044 for an isolated crystal to 0.736 for a simple chain (Fig. 10a; Table 2). For five parallel chains of giant bullets, our simulation gives $M_{rs}=0.48$ (Fig. 10b), as expected for this geometry. Results for a linear chain of three spearhead crystals (Fig. 10c) also have increased M_{rs} compared to a single spearhead (Table 2). Modelling multiple parallel chains of spearhead crystals (Fig. 10d) indicates a further increase in M_{rs} (Table 2), although parallel strands of magnetosomes are not likely to represent a mechanically stable arrangement (e.g., Hanzlik et al., 2002).

Overall, our modelling results indicate that giant bullets have increased M_{rs} in linear chains because of positive magnetic interactions, and decreased M_{rs} in parallel chains, as expected. On the other hand, multi-stranded chains of spindle and spearhead crystals have increased M_{rs}. This is not expected because parallel chains generally tend to reduce M_{rs} due to negative magnetic interactions. The increased M_{rs} is due to the crystal geometry of spindles and spearheads at their highly tapered ends, which results in stray fields that encourage nucleation of a SD state. It is the magnetic-to-thermal energy that is crucial for magnetotaxis, so giant magnetofossil crystals in the PSD state may have sufficient magnetic moment for magnetotaxis even with small M_{rs} values. Likewise, particle elongation along the $<1\,0\,0>$ direction in magnetite is considered non-ideal for magnetotaxis. However, magnetotactic organisms do not always optimize biomineralization for magnetotaxis, as was first realized by Vali and Kirschvink (1991) who reported grains elongated along the $<1\,0\,0>$ direction in a magnetotactic bacterium. The fact that SD structures are obtained for some giant magnetite crystals in chain configurations does not necessarily indicate that they were used for magnetotaxis. The purpose of our modelling is to demonstrate the enhancement to SD structure when aligned in different chain configurations compared to the apparent PSD/MD structures of isolated crystals. These results suggest that the particles in question could have been used for magnetotaxis if they were configured in the modelled optimal chain configurations. It should also be noted that exposure to magnetic fields (e.g., during magnetic extraction) can promote alignment into chains, and metastable SD structures (Kobayashi et al., 2006).

The navigation hypothesis for some configurations of giant crystals is also supported by detailed crystallographic observations. TEM analyses of needle-like crystals consistently indicate that crystal elongation is along the $<1\,1\,1>$ direction (Fig. 6), which is the easy axis of magnetization for magnetite. Elongation along this direction is considered to enhance magnetotaxis, although this enhancement is small compared to that produced by increasing grain elongation and chain alignment. This is consistent with natural selection promoting maximum magnetic moments that maximize magnetotaxis efficiency. In contrast, morphologies with MD magnetic structures (either as single crystals or in chains) probably had non-magnetic functions. Schumann et al. (2008) argued that such giant magnetic crystals might have been used for hardening, as is the case for chiton teeth (Lowenstam, 1962), or that they served a structural purpose such as protective armouring.

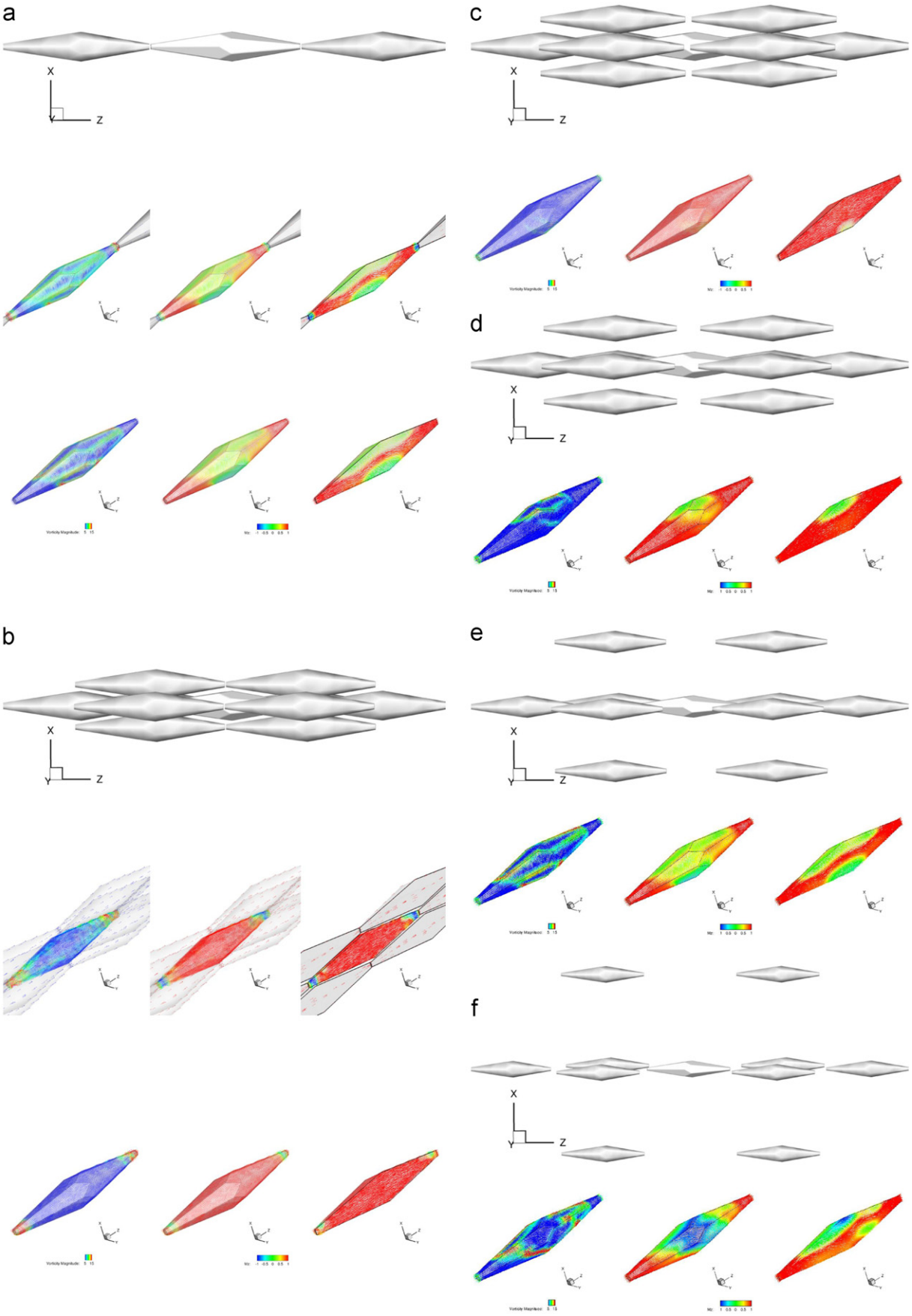

Fig. 9. Micromagnetic model results for different chains of spindle-like magnetite crystals using a constrained optimization method. (a) A linear chain with three spindles (2.245×0.375 μm). (b-f) Multiple parallel chains of eleven spindles (2.245×0.375 μm) with different inter-particle spacings ranging from 0.02 to 2.5 μm (geometries are shown at the top of each sub-figure). Magnetic domain structures are plotted as described in Fig. 8. The results indicate enhancement to SD structure for the spindles with decreasing inter-particle spacing when aligned in multi-stranded chains.

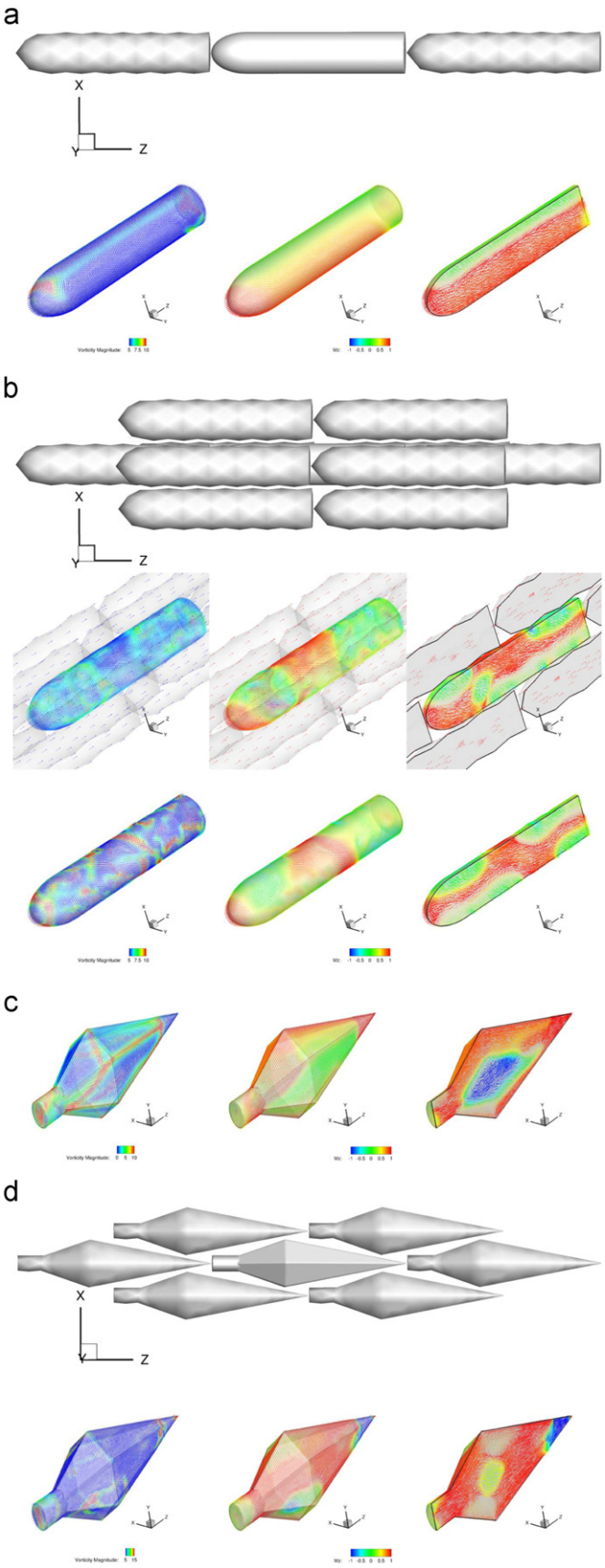

Fig. 10. Micromagnetic model results for different chains of giant bullet-shaped magnetite crystals using a constrained optimization method. (a) A linear chain with three giant bullets (2.081 × 0.478 μm). (b) Multiple parallel chains of eleven giant bullets (2.081 × 0.478 μm) with an inter-particle gap of 0.02 μm (geometries are shown at the top of each sub-figure). Magnetic domain structures are plotted as described in Fig. 8. Our modelling results indicate that bullet-shaped crystals have higher M_{rs} when aligned in linear chains and lower M_{rs} in parallel chains. (c-d) Micromagnetic model results for different chains of spearhead magnetite crystals using a constrained optimization method. (c) A linear chain with three spearheads (3.300 × 0.513 μm). (d) Multiple parallel chains of seven spearheads (3.300 × 0.513 μm) with an inter-particle gap of 0.02 μm (particle configuration at the top). The magnetic domain structures are plotted as described in Fig. 8. Our results indicate enhancement to a SD structure when spearheads are aligned in multi-stranded chains.

Table 2
Micromagnetic modelling results for chains of giant magnetofossils.

Geometry	Size (μm)	Inter-grain gap (μm)	Normalized M_{rs}
Single spindle	2.245 × 0.375	N/A	0.355
3 × Spindles	2.245 × 0.375	0.02	0.505
11 × Spindles	2.245 × 0.375	0.02	0.982
11 × Spindles	2.245 × 0.375	0.10	0.969
11 × Spindles	2.245 × 0.375	0.40	0.856
11 × Spindles	2.245 × 0.375	1.00	0.499
11 × Spindles	2.245 × 0.375	2.50	0.441
Single giant bullet	2.081 × 0.478	N/A	0.025
3 × giant bullets	2.081 × 0.478	0.02	0.736
11 × giant bullets	2.081 × 0.478	0.02	0.486
Single spearhead	3.300 × 0.513	N/A	0.005
3 × Spearheads	3.300 × 0.513	0.02	0.266
7 × Spearheads	3.300 × 0.513	0.02	0.743

5. Conclusions

In addition to one previous report of giant magnetofossils in a coastal setting from the North Atlantic Ocean (Schumann et al., 2008), we have identified giant magnetofossils in deep-sea environments from the Southern Ocean and equatorial Indian Ocean. Discovery of morphologically identical giant magnetofossils in both hemispheres indicates that the organisms in question had widespread distribution. Further studies are needed to determine their full geographic extent, although it was probably global. The only previous report of giant magnetofossils (Schumann et al., 2008) suggested that they only occurred during the PETM. We find giant biogenic magnetite not only during (Fig. 4), but also before (Fig. 5) and after the PETM (Fig. 6). Increased global temperatures associated with the PETM, and enhanced weathering, therefore, cannot be the only factors that promoted biomineralization of such giant magnetite crystals, although hyperthermal conditions probably significantly enhanced their gigantism. While giant magnetofossil occurrences are not associated uniquely with peak global temperatures during hyperthermals, our identification of previously unknown giant bullet-shaped magnetite during the MECO event provides a further general connection between giant magnetofossils and hyperthermal events. Enhanced global weathering during hyperthermals, and expanded suboxic diagenetic zones within sediments, probably provided more bioavailable iron to pelagic marine environments, which eased a key limiting factor for magnetite biomineralization and enabled growth of giant magnetofossils. Micromagnetic simulation indicates that giant magnetofossils can have either SD or MD structures depending on their size, shape and arrangement in chain structures. Such giant magnetite crystals probably had different functions, including magnetotaxis, protective, and structural purposes. Modelled SD structures for some giant crystals and chains, and elongation along the $<1\,1\,1>$ crystallographic axis of needle-like magnetite crystals, supports the interpretation that some giant magnetofossil morphologies may have been used for magnetotaxis.

Acknowledgements

Samples were provided by the IODP, which is sponsored by the U.S. National Science Foundation and participating countries under management of Joint Oceanographic Institutions, Inc. We thank Shane Paxton for assistance with magnetic separation, and Paul Hesse and Mark Hounslow for useful discussions about preparing TEM samples. We are grateful to Michael Winklhofer and Joseph Kirschvink for comments that significantly improved this paper, and to Jean Lynch-Stieglitz for editorial handling. This work was partially supported by U.K. Natural Environment Research Council grant NE/G003319/1 to APR, WW, and ARM, and Spanish MEC grant PR2011–0480 to JCL.

References

Abraçado, L.G., Abreu, F., Keim, C.N., Campos, A.P., Lins, U., Farina, M., 2010. Magnetosome chain superstructure in uncultured magnetotactic bacteria. Phys. Biol. 7, 046016.
Bazylinski, D.A., Frankel, R.B., 2004. Magnetosome formation in prokaryotes. Nature Rev. Microbiol. 2, 217–230.
Bohaty, S.M., Zachos, J.C., 2003. A significant Southern Ocean warming event in the late middle Eocene. Geology 31, 1017–1020.
Bowen, G.J., Beerling, D.J., Koch, P.L., Zachos, J.C., Quattlebaum, T., 2004. A humid climate state during the Paleocene/Eocene thermal maximum. Nature 432, 495–499.
Buseck, P.R., Dunin-Borkowski, R.E., Devouard, B., Frankel, R.B., McCartney, M.R., Midgley, P.A., Posfai, M., Weyland, M., 2001. Magnetite morphology and life on Mars. Proc. Natl. Acad. Sci. USA 98, 13490–13495.
Cramer, B.S., Kent, D.V., 2005. Bolide summer: the Paleocene/Eocene thermal maximum as a response to an extraterrestrial trigger. Palaeogeogr. Palaeoclimatol. Palaeoecol. 224, 144–166.
Fletcher, E.J., O'Reilly, W., 1974. Contribution of Fe^{2+} ions to the magnetocrystalline anisotropy constant K_1 of $Fe_{3-x}Ti_xO_4$ ($0 < x < 0.1$). J. Phys. C 7, 171–178.
Flies, C.B., Jonkers, H.M., de Beer, D., Bosselmann, K., Böttcher, M.E., Schüler, D., 2005. Diversity and vertical distribution of magnetotactic bacteria along chemical gradients in freshwater microcosms. FEMS Microbiol. Ecol. 52, 185–195.
Hanzlik, M., Winklhofer, M., Petersen, N., 2002. Pulsed-field remanence measurements on individual magnetotactic bacteria. J. Magn. Magn. Mater. 248, 258–267.
Heider, F., Williams, W., 1988. Note on temperature dependence of exchange constant in magnetite. Geophys. Res. Lett. 15, 184–187.
Hesse, P.P., 1994. Evidence for bacterial palaeoecological origin of mineral magnetic cycles in oxic and sub-oxic Tasman Sea sediments. Mar. Geol. 117, 1–17.
Jovane, L., Florindo, F., Coccioni, R., Dinarès-Turell, J., Marsili, A., Monechi, S., Roberts, A.P., Sprovieri, M., 2007. The middle Eocene climatic optimum (MECO) event in the Contessa Highway section, Umbrian Appenines, Italy. Geol. Soc. Am. Bull. 119, 413–427.
Katzmann, E., Müller, F., Lang, C., Messerer, M., Winklhofer, M., Plitzko, J.M., Schüler, D., 2011. Magnetosome chains are recruited to cellular division sites and split by asymmetric septation. Mol. Microbiol. 82, 1316–1329.
Kennett, J.P., Stott, L.D., 1991. Abrupt deep-sea warming, palaeoceanographic changes and benthic extinctions at the end of the Paleocene. Nature 353, 225–229.
Kent, D.V., Cramer, B.S., Lanci, L., Wang, D., Wright, J.D., Van der Voo, R., 2003. A case for a comet impact trigger for the Paleocene/Eocene thermal maximum and carbon isotope excursion. Earth Planet. Sci. Lett. 211, 13–26.
Kobayashi, A., Kirschvink, J.L., Nash, C.Z., Kopp, R.E., Sauer, D.A., Bertani, L.E., Voorhout, W.F., Taguchi, T., 2006. Experimental observation of magnetosome chain collapse in magnetotactic bacteria: sedimentological, paleomagnetic, and evolutionary implications. Earth Planet. Sci. Lett. 245, 538–550.
Kopp, R.E., Kirschvink, J.L., 2008. The identification and biogeochemical interpretation of fossil magnetotactic bacteria. Earth Sci. Rev. 86, 42–61.
Kopp, R.E., Raub, T.D., Schumann, D., Vali, H., Smirnov, A.V., Kirschvink, J.L., 2007. Magnetofossil spike during the Paleocene-Eocene thermal maximum: ferromagnetic resonance, rock magnetic, and electron microscopy evidence from Ancora, New Jersey, United States. Paleoceanography 22, PA4103, http://dx.doi.org/10.1029/2007PA001473.
Kopp, R.E., Schumann, D., Raub, T.D., Powars, D.S., Godfrey, L.V., Swanson-Hysell, N.L., Maloof, A.C., Vali, H., 2009. An Appalachian Amazon? Magnetofossil evidence for the development of a tropical river-like system in the mid-Atlantic United States during the Paleocene-Eocene Thermal Maximum. Paleoceanography 24, PA4211, http://dx.doi.org/10.1029/2009PA001783.
Larrasoaña, J.C., Roberts, A.P., Chang, L., Schellenberg, S.A., Fitz Gerald, J.D., Norris, R.D., Zachos, J.C., 2012. Magnetotactic bacterial response to Antarctic dust supply during the Paleocene-Eocene thermal maximum. Earth Planet. Sci. Lett. 333–334, 122–133.
Li, J.H., Pan, Y.X., Liu, Q.S., Zhang, K.Y., Menguy, N., Che, R.C., Qin, H.F., Lin, W., Wu, W.F., Petersen, N., Yang, X., 2010. Biomineralization, crystallography and magnetic properties of bullet-shaped magnetite magnetosomes in giant rod magnetotactic bacteria. Earth Planet. Sci. Lett. 293, 368–376.
Lins, U., et al., 2007. Magnetite (Fe_3O_4) and greigite (Fe_3S_4) crystals in multicellular magnetotactic prokaryotes. Geomicrobiol. J. 24, 43–50.
Lippert, P.C., Zachos, J.C., 2007. A biogenic origin for anomalous fine-grained magnetic material at the Paleocene-Eocene boundary at Wilson Lake, New Jersey. Paleoceanography 22, PA4104, http://dx.doi.org/10.1029/2007PA001471.
Lowenstam, H.A., 1962. Magnetite in denticle capping in recent chitons (*Polyplacophora*). Geol. Soc. Am. Bull. 73, 435–438.
Mann, S., Moench, T.T., Williams, R.J.P., 1984. A high resolution electron microscopic investigation of bacterial magnetite. Implications for crystal growth. Proc. R. Soc. Lond. B 221, 385–393.
Matsuda, T., Endo, J., Osakabe, N., Tonomura, A., Arii, T., 1983. Morphology and structure of biogenic magnetite particles. Nature 302, 411–412.

Muxworthy, A.R., Williams, W., 2006. Critical single-domain/multi-domain grain sizes in noninteracting and interacting elongated magnetite particles: implications for magnetosomes. J. Geophys. Res. 111, B12S12, http://dx.doi.org/10.1029/2006JB004588.

Petersen, N., von Dobeneck, T., Vali, H., 1986. Fossil bacterial magnetite in deep-sea sediments from the South Atlantic Ocean. Nature 320, 611–614.

Roberts, A.P., Florindo, F., Villa, G., Chang, L., Jovane, L., Bohaty, S.M., Larrasoaña, J.C., Heslop, D., Fitz Gerald, J.D., 2011. Magnetotactic bacterial abundance in pelagic marine environments is limited by organic carbon flux and availability of dissolved iron. Earth Planet. Sci. Lett. 310, 441–452.

Roberts, A.P., Chang, L., Heslop, D., Florindo, F., Larrasoaña, J.C., 2012. Searching for single domain magnetite in the 'pseudo-single-domain' sedimentary haystack: implications of biogenic magnetite preservation for sediment magnetism and relative paleointensity determinations. J. Geophys. Res. 117, B08104, http://dx.doi.org/10.1029/2012JB009412.

Schrefl, T., 1999. Finite elements in numerical micromagnetics Part I: Granular hard magnets. J. Magn. Magn. Mater. 207, 45–65.

Schumann, D., et al., 2008. Gigantism in unique biogenic magnetite at the Paleocene–Eocene Thermal Maximum. Proc. Natl. Acad. Sci. USA 105, 17648–17653.

Sluijs, A., et al., 2007. Environmental precursors to rapid light carbon injection at the Paleocene/Eocene boundary. Nature 450, 1218–1221.

Stoltz, J.F., Chang, S.B.R., Kirschvink, J.L., 1986. Magnetotactic bacteria and single-domain magnetite in hemipelagic sediments. Nature 321, 849–851.

Tarduno, J.A., Wilkison, T.W., 1996. Non-steady state magnetic mineral reduction, chemical lock-in, and delayed remanence acquisition in pelagic sediments. Earth Planet. Sci. Lett. 144, 315–326.

Vali, H., Kirschvink, J.L., 1989. Magnetofossil dissolution in a palaeomagnetically unstable deep-sea sediment. Nature 339, 203–206.

Vali, H., Kirschvink, J.L., 1991. Observations of magnetosome organization, surface structure, and iron biomineralization of undescribed magnetic bacteria: evolutionary speculations. In: Frankel, R.P., Blakemore, R.P. (Eds.), Iron Biomineralization. Plenum Press, New York, pp. 97–115.

Williams, W., Muxworthy, A.R., Paterson, G.A., 2006. Configurational anisotropy in single-domain and pseudo-single-domain grains of magnetite. J. Geophys. Res. 111, B12S13, http://dx.doi.org/10.1029/2006JB004556.

Williams, W., Evans, M.E., Krása, D., 2010. Micromagnetics of paleomagnetically significant mineral grains with complex morphology. Geochem. Geophys. Geosyst. 11, Q02Z14, http://dx.doi.org/10.1029/2009GC002828.

Zachos, J.C., Dickens, G.R., Zeebe, R.E., 2008. An early Cenozoic perspective on greenhouse warming and carbon-cycle dynamics. Nature 451, 279–283.